Cohesion promotes nucleolar structure and function

Bethany Harris[a], Tania Bose[a], Kenneth K. Lee[a], Fei Wang[a], Shuai Lu[a,b], Rhonda Trimble Ross[a], Ying Zhang[a], Sarah L. French[c], Ann L. Beyer[c], Brian D. Slaughter[a], Jay R. Unruh[a], and Jennifer L. Gerton[a,b]

[a]Stowers Institute for Medical Research, Kansas City, MO 64110; [b]Department of Biochemistry and Molecular Biology, University of Kansas Medical Center, Kansas City, KS 66160; [c]Department of Microbiology, Immunology and Cancer Biology, University of Virginia School of Medicine, Charlottesville, VA 22908

ABSTRACT The cohesin complex contributes to ribosome function, although the molecular mechanisms involved are unclear. Compromised cohesin function is associated with a class of diseases known as cohesinopathies. One cohesinopathy, Roberts syndrome (RBS), occurs when a mutation reduces acetylation of the cohesin Smc3 subunit. Mutation of the cohesin acetyltransferase is associated with impaired rRNA production, ribosome biogenesis, and protein synthesis in yeast and human cells. Cohesin binding to the ribosomal DNA (rDNA) is evolutionarily conserved from bacteria to human cells. We report that the RBS mutation in yeast (*eco1-W216G*) exhibits a disorganized nucleolus and reduced looping at the rDNA. RNA polymerase I occupancy of the genes remains normal, suggesting that recruitment is not impaired. Impaired rRNA production in the RBS mutant coincides with slower rRNA cleavage. In addition to the RBS mutation, mutations in any subunit of the cohesin ring are associated with defects in ribosome biogenesis. Depletion or artificial destruction of cohesion in a single cell cycle is associated with loss of nucleolar integrity, demonstrating that the defects at the rDNA can be directly attributed to loss of cohesion. Our results strongly suggest that organization of the rDNA provided by cohesion is critical for formation and function of the nucleolus.

INTRODUCTION

The cohesin complex forms a ring that interacts with chromatin at many different locations in the genome. These interactions are important for DNA replication, segregation, organization, condensation, repair, and gene expression. The complex, composed of four subunits—Smc1, Smc3, Scc3, and Mcd1/Scc1—is regulated by the acetylation activity of Eco1 and the loading activity of Scc2. Mutations in cohesin affect the clustering of some sequences, such as

telomeres, but not centromeres, despite cohesin's association with centromeres (Gard *et al.*, 2009). One method by which cohesin may contribute to gene expression is through the localization of cohesin-bound genes, such as *GAL2*, to the nuclear periphery upon transcriptional activation in budding yeast (Gard *et al.*, 2009). Long-distance interactions between sequences depend on cohesin, which could also influence their expression (Bose and Gerton, 2010; Kirkland and Kamakaka, 2013). Cohesin contributes to chromosome condensation, including the condensation of the ribosomal DNA (rDNA) in budding yeast (Guacci *et al.*, 1997; Gard *et al.*, 2009; Heidinger-Pauli *et al.*, 2010). Thus cohesin and its regulators are important for organization of cohesin-associated regions in the nucleus. The association of cohesin with the rDNA repeats is evolutionarily conserved from bacteria to human cells, making rDNA an interesting locus at which to understand cohesin's contribution to rDNA function.

Acetylation of the Smc3 subunit of the cohesin complex by Eco1 locks the ring, making it cohesive (Rolef Ben-Shahar *et al.*, 2008; Unal *et al.*, 2008). In addition to the cohesin complex, Eco1 can acetylate Mps3, a subunit of the spindle pole body (SPB). Mutations that block acetylation left SPB duplication intact but reduced sister chromatid cohesion, telomere tethering, and insertion of Mps3 into the nuclear envelope (Ghosh *et al.*, 2012), suggesting that

Abbreviations used: 3C, chromosome conformation capture; ChIP, chromatin immunoprecipitation; DAPI, 4′,6-diamidino-2-phenylindole; dNSAF, normalized spectral abundance factor; EM, electron microscopy; FISH, fluorescent in situ hybridization; GFP, green fluorescent protein; KS, Kolmogorov–Smirnov; MudPIT, multidimensional protein identification technology; pol, polymerase; qPCR, quantitative PCR; RBS, Roberts syndrome; rDNA, ribosomal DNA; RFP, red fluorescent protein; SPB, spindle pole body; TAP, tandem affinity purification; TEV, tobacco etch virus; WT, wild type; YPD, yeast extract/peptone/dextrose.

additional targets of Eco1 could influence nuclear function. Mutations that disrupt the acetyltransferase activity of ESCO2, one of the two human homologues of *ECO1*, are associated with Roberts syndrome (RBS; Vega *et al.*, 2005). Heterochromatic repulsion, one hallmark of metaphase chromosomes derived from RBS cells, includes both centromere and rDNA sequences. The appearance of these heterochromatic regions suggests that they lack cohesion. A mutation in the acetyltransferase domain of *ECO1* in budding yeast (*eco1-W216G*) disrupts cohesion at the rDNA as well as nucleolar morphology (Gard *et al.*, 2009; Bose *et al.*, 2012). These defects in both yeast and human cells correlate with decreased rRNA production and lower ribosome function (Bose *et al.*, 2012). *ECO1* may influence nuclear processes through its effect on cohesin as well as other targets, but the disruption of cohesion at the rDNA in both yeast and human cells in acetyltransferase mutants suggests that this will be an important phenotype to understand.

The nucleolus is the cellular organelle responsible for ribosome production. Organization within the nucleolus is critical for its efficient function (Nemeth and Langst, 2011). RBS cells have highly fragmented nucleoli, consistent with a loss of nucleolar function (Xu *et al.*, 2013). Within the single budding yeast nucleolus, RNA polymerase I transcribes about half of the 100–200 rDNA repeats. Loops form in the rDNA, which may be important for transcription reinitiation (Mayan and Aragon, 2010). Understanding the factors that contribute to the efficient transcription of the rDNA repeats is critical because it is the most highly transcribed locus in a cell, and the assembly of ribosomes can be limited by the level of rRNA (Laferte *et al.*, 2006). Furthermore, defects in ribosome function are associated with a group of human diseases known as ribosomopathies (Narla and Ebert, 2010). We address how cohesion contributes to nucleolar function. We find that cohesion is necessary for 35S and 5S gene loop formation and the integrity of the nucleolus.

RESULTS AND DISCUSSION

RNA polymerase I levels and stoichiometry are normal in the *eco1-W216G* mutant

One possible mechanism for poor rRNA production is a low level of RNA polymerase I. Given the major gene expression changes associated with the *eco1-W216G* mutant (Bose *et al.*, 2012), we compared the levels of RNA polymerase I to that in wild-type (WT) cells. Reduced RNA pol I in the mutant cells could explain the lower level of transcript observed. RNA pol I is composed of 14 subunits. We used Western blotting to determine that WT and mutant cells had similar levels of the large subunit, Rpa190, indicating no significant defect in protein level (Figure 1A). Furthermore, we purified RNA pol I via Rpa190 from both the mutant and WT strain and could not detect any differences in composition by either silver stain or semiquantitative proteomic analysis (Figure 1, B and C). Because the *eco1-W216G* mutant had normal RNA pol I levels and no difference in the stoichiometry of the subunits, a simple reduction in the amount of RNA pol I is not likely to explain the transcriptional defect at the rDNA in the mutant. It has been suggested that cohesin facilitates the transition from paused RNA polymerase II to an elongating form at active genes in *Drosophila melanogaster* (Schaaf *et al.*, 2013). We decided to further investigate the behavior of RNA polymerase I in the *eco1-W216G* mutant background.

rRNA transcription and cleavage are defective in the eco1-W216G mutant

The 35S transcript is made as a single transcript by RNA polymerase I and then cleaved and modified by a host of RNAs and proteins termed the processome to make the final 18S, 5.8S, and 25S RNAs, which are assembled with protein components of the 40S and 60S ribosomal subunits. We previously used two independent methods, metabolic labeling and fluorescent in situ hybridization (FISH), to show that the production of rRNA was reduced in the *eco1-W216G* mutant background as compared with WT, and ribosome biogenesis was impaired (Bose *et al.*, 2012). Production of rRNA transcripts can be regulated at many levels, including polymerase recruitment, elongation, processing, and decay. Because rRNA cleavage occurs both during and after elongation (Osheim *et al.*, 2004; Schneider *et al.*, 2007; Kos and Tollervey, 2010), we postulated that cleavage would be delayed in the mutant if the production defect was after polymerase recruitment.

Cells were pulse labeled for 2 min with [^{3}H]methyl-methionine and then chased with cold methionine for 0, 2, 5, or 15 min. The [^{3}H] methyl group acts as a donor for rRNA methylation, so transcripts in any phase of transcription can be labeled (unless they are already fully methylated). RNA was isolated and the various forms compared (Figure 2A). In the *eco1-W216G* mutant, the persistence of the 35S transcript labeled during the pulse is apparent at 2 and 5 min. In rapid labeling kinetic experiments, the 35S gene took <3 min to be synthesized and processed (Kos and Tollervey, 2010), so the observed delay is significantly longer than the normal time. Furthermore, more of the precleaved 27S form persists at the 5-min time point in the mutant relative to the WT strain. We conclude that cleavage of the 35S transcript occurs more slowly in the *eco1-W216G* strain and that the production defect is at least partly after polymerase recruitment.

We previously showed that the *eco1-W216G* mutation does not affect rDNA array size or percentage of active genes (Bose *et al.*, 2012). Given the lower rates of rRNA production in the *eco1-W216G* strain, we asked whether we would detect a decrease in RNA pol I association with the 35S gene by chromatin immunoprecipitation (ChIP). Surprisingly, we found an increased association of RNA pol I at both the promoter region (primer pair 4) and across the body of the 35S gene (primers pairs 7–14) in the *eco1-W216G* mutant (Figure 2B). This increase was statistically significant for every primer pair—even the *TUB1* locus that was used as a negative control. The signal at the *TUB1* locus was very low relative to the signal at the 35S gene, as expected. The difference in signal between the mutant and WT samples may be explained in part by the increase in nuclear–nucleolar overlap in the *eco1-W216G* mutant, which could allow RNA pol I to cross-link to the *TUB1* locus at a low level (see later discussion). These results suggest that recruitment of RNA pol I to the rDNA repeats is not compromised in the *eco1-W216G* mutant background.

The ChIP signal is displayed as IP/input, which should eliminate any bias in repeat recovery in the fractionation procedure. Nevertheless, we decided to further investigate the behavior of the rDNA repeats in chromatin fractionation. If the rDNA repeats were not partitioning normally in standard chromatin fractionation procedures in the mutant strain, our interpretation of the ChIP results might need to be adjusted. Chromatin fractionation was carried out after cross-linking in order to assess the behavior of the rDNA repeats in low- and high-speed centrifugation (Rougemaille *et al.*, 2008). Normal ChIP fractionation procedure recovers the soluble high-speed fraction. We quantified the amount of rDNA in the fractions by quantitative PCR (qPCR) and found very similar levels of rDNA in the high-speed supernatant fraction used for ChIP (Figure 2C), suggesting that differential fractionation of rDNA sequences cannot explain the difference in ChIP signal in mutant versus WT.

Miller spreads were used as a measure of polymerase occupancy on rDNA genes (Figure 2D). We did not observe significant changes
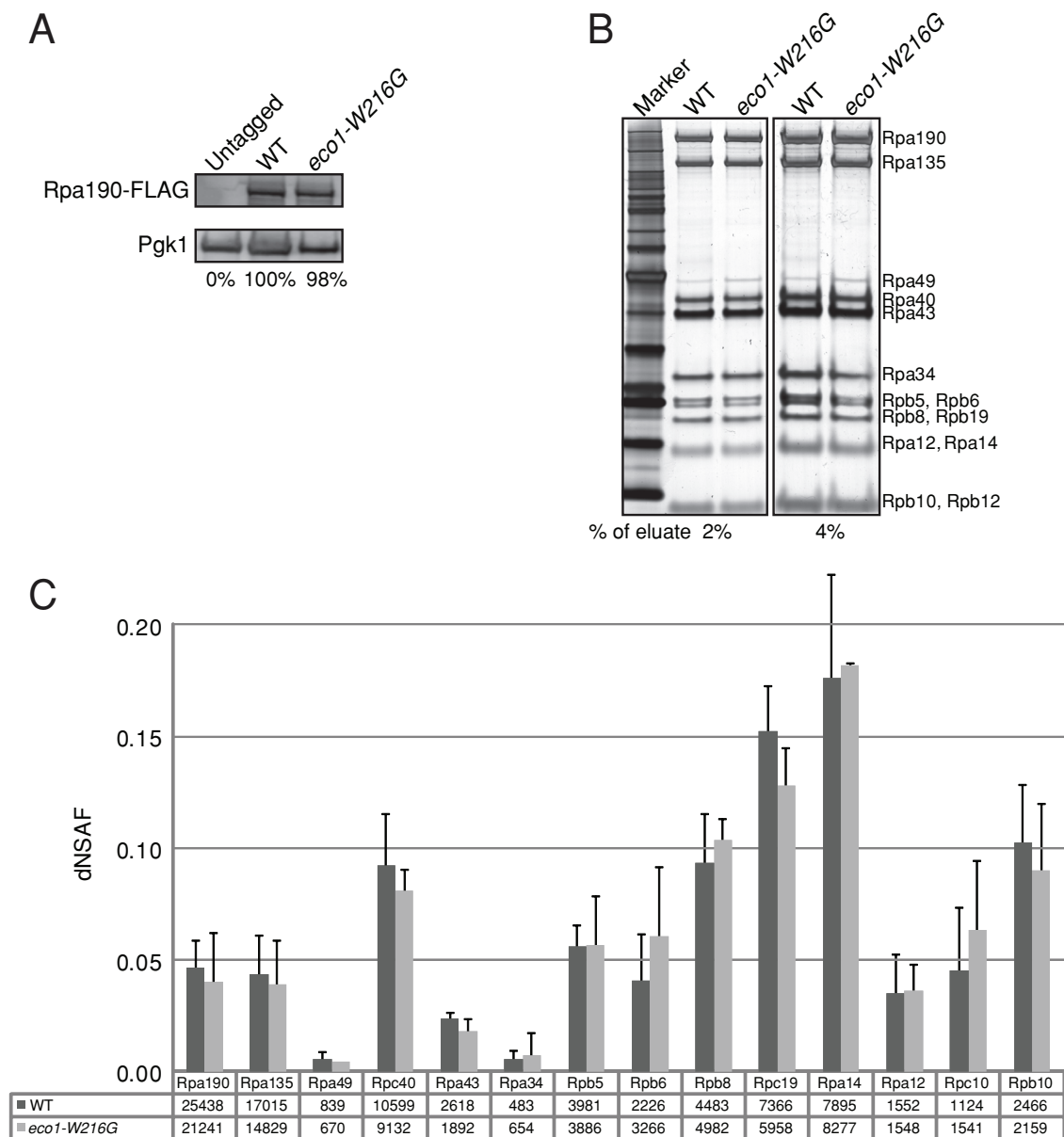
FIGURE 1: RNA polymerase I levels are not altered in the *eco1-W216G* mutant background. (A) For the Western blot, equal amounts of protein from whole-cell extracts were loaded to monitor Rpa190-FLAG. Pgk1 was used as a loading control. The level of Rpa190 is shown as a percentage of the Pgk1 signal. (B) After tandem affinity purification (TAP) of Rpa190 in WT and *eco1-W216G* mutant strains, either 2 or 4% of the eluate was loaded onto a polyacrylamide gel and silver stained. The identity of the bands is inferred from their migration. (C) The TAP-purified material was subjected to MudPIT analysis. dNSAF values were calculated based on the spectral counts for two biological replicates (merged spectral counts shown below each subunit) and the size of the protein (Zhang *et al.*, 2010). Error bars, SD.

	Rpa190	Rpa135	Rpa49	Rpc40	Rpa43	Rpa34	Rpb5	Rpb6	Rpb8	Rpc19	Rpa14	Rpa12	Rpc10	Rpb10
WT	25438	17015	839	10599	2618	483	3981	2226	4483	7366	7895	1552	1124	2466
eco1-W216G	21241	14829	670	9132	1892	654	3886	3266	4982	5958	8277	1548	1541	2159

in the number of polymerases per active repeat in the *eco1-W216G* mutant strain as compared with WT in either the W303a or BY4742 background, consistent with the ChIP results showing no decrease in RNA pol I association. The different results in the ChIP and Miller spread assays may be due to differences in gene accessibility to the experimental technique, the presence (ChIP) or absence (Miller) of cross-linking, or other biases we do not understand. However, in neither case do we observe significantly less RNA pol I at the rDNA in the mutant, so we conclude that lower levels of recruitment of RNA pol I are unlikely to contribute to the transcriptional defect at the locus.

Mutations that decrease the number of polymerases per repeat include mutations that affect RNA pol I. Deletion of the nonessential Rpa49 subunit results in significantly reduced polymerase occupancy on rDNA genes (Beckouet *et al.*, 2008; Albert *et al.*, 2011). We compared steady-state distributions of RNA produced from a single rDNA repeat using FISH (Tan and van Oudenaarden, 2010) in the *eco1-W216G* and the *rpa49Δ* mutants. Whereas RNA pol I levels at the rDNA are compromised in the *rpa49Δ* but not the *eco1-W216G* mutant, both mutants had similar reductions in rRNA production by FISH (Figure 2E). If we assume that the decay rate is similar in all three strains, we can calculate a transcriptional burst size.
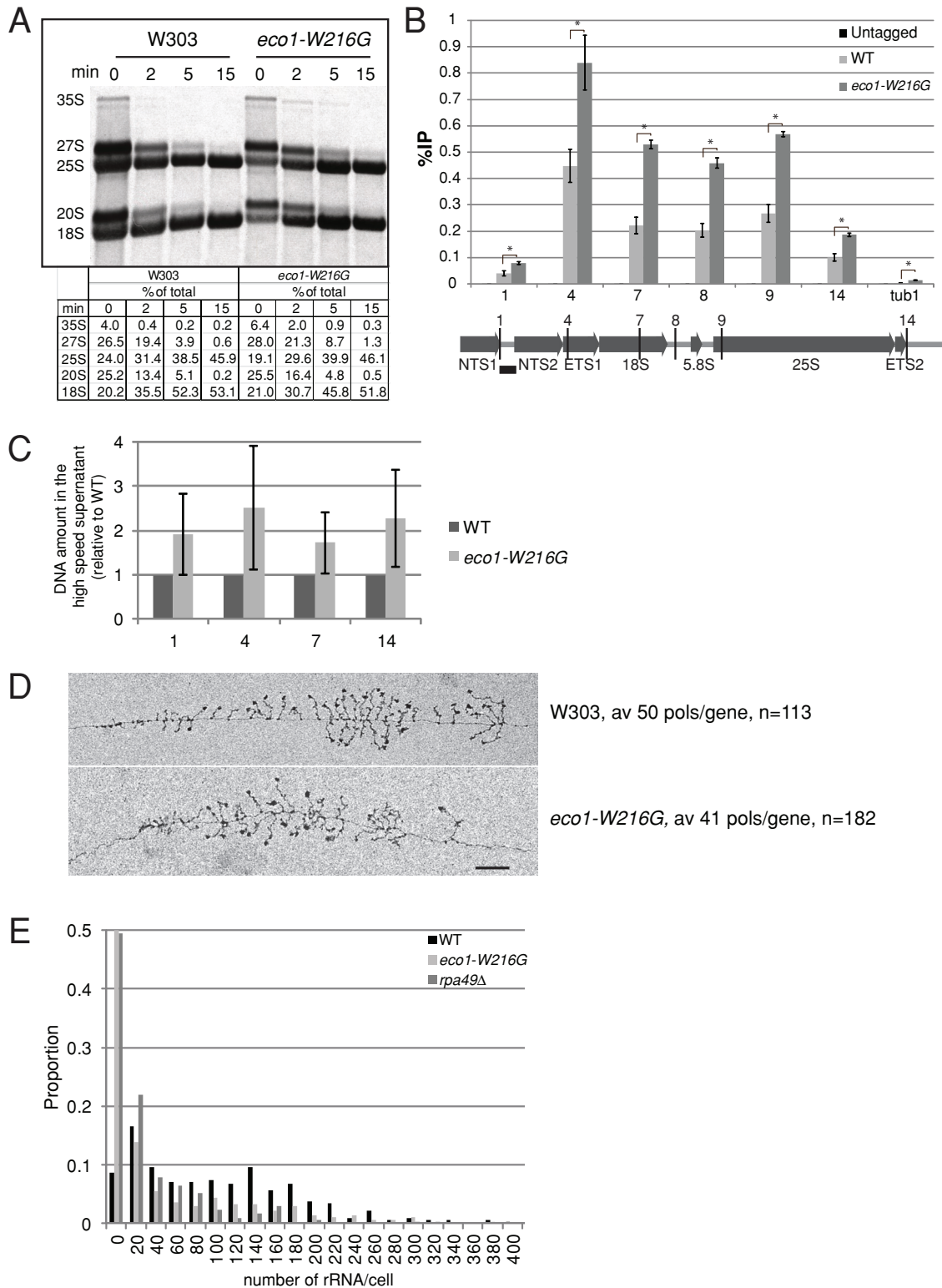
FIGURE 2: Evaluation of RNA polymerase 1 in the *eco1-W216G* mutant background suggests that elongation is impaired. (A) Equal numbers of WT and mutant cells were pulse labeled for 2 min with [³H]methyl-methionine, and then chased with cold methionine for various times as indicated. RNA was isolated, and equal counts were loaded per lane in order to more easily compare cleavage products. 25S and 18S represent the final form of the 35S transcript. 27S and 20S are cleavage intermediates. 35S and 27S products persist in the mutant background. (B) ChIP was performed for Rpa190-FLAG in the WT and *eco1-W216G* mutant backgrounds. qPCR was used to monitor several DNA sequences, as indicated. The black bar below the schematic of the rDNA indicates the region of cohesin binding. Percentage IP was calculated by dividing the mean value for the immunoprecipitated sample by the mean value from the input. Two biological replicates were done, each with two technical replicates, and each technical replicate was used in three

Panel A data table:

	W303 % of total				eco1-W216G % of total			
min	0	2	5	15	0	2	5	15
35S	4.0	0.4	0.2	0.2	6.4	2.0	0.9	0.3
27S	26.5	19.4	3.9	0.6	28.0	21.3	8.7	1.3
25S	24.0	31.4	38.5	45.9	19.1	29.6	39.9	46.1
20S	25.2	13.4	5.1	0.2	25.5	16.4	4.8	0.5
18S	20.2	35.5	52.3	53.1	21.0	30.7	45.8	51.8

We find 247 ± 14 molecules/burst for WT, 80.1 ± 5.6 for *eco1-W216G*, and 77.2 ± 8.7 for *rpa49Δ*. Thus it seems that different mechanisms can contribute to a similar reduction in the production of rRNA. Although the recruitment of RNA pol I to the repeats seems normal in the *eco1-W216G* mutant, the slower cleavage of rRNA, combined with the higher cross-linking of RNA pol I, suggests that the rate of elongation by RNA pol I may be compromised in the *eco1-W216G* mutant, but this will require further experiments.

Nucleolar structure in the eco1-W216G mutant is aberrant

A nucleolar defect in the *eco1-W216G* mutant was previously reported, based on indirect immunofluorescence for a nucleolar protein (Gard *et al.*, 2009). We wanted to examine the nucleolar structure more directly and at higher resolution using electron microscopy (EM). The nucleoli in the *eco1-W216G* mutant cells were disrupted, with many nucleoli having an ill-defined border (Figure 3A). We compared the appearance of the nucleoli in the *eco1-W216G* mutant to an *rpa49Δ* mutant, which was previously shown to have defects in nucleolar structure (Albert *et al.*, 2011). The nucleoli in the *rpa49Δ* mutant also tended to be irregularly shaped. In addition, several nucleoli in the *rpa49Δ* mutant were detached from the nuclear periphery, a phenotype never observed in WT or *eco1-W216G* mutant cells.

We used a fluorescent reporter, Sik1–red fluorescent protein (RFP), to demonstrate that the nucleolar signal in the *eco1-W216G* mutant displayed significantly more overlap with the bulk chromatin (4′,6-diamidino-2-phenylindole [DAPI]; Figure 3B), as might be expected based on EM and previous analysis (Gard *et al.*, 2009). The EM and fluorescence experiments demonstrate that nucleolar integrity is compromised in the *eco1-W216G* mutant. Consistent with these observations in budding yeast, there is a high degree of nucleolar fragmentation in human RBS cells (Xu *et al.*, 2013), suggesting that ESCO2 may be especially important for organization of the rDNA repeats in human cells. The comparison between the phenotypes of the *rpa49Δ* and *eco1-W216G* mutants demonstrates that mutations that are expected to act through distinct mechanisms can have similar effects on rRNA production and nucleolar morphology.

The 35S and 5S genes form loops that can be detected by chromosome conformation capture (3C; Mayan and Aragon, 2010). These loops have been proposed to facilitate transcription reinitiation. Given that cohesin binds to the nontranscribed region of the rDNA (Laloraya *et al.*, 2000), we speculated that the gene loops depend on cohesin. We investigated cross-linking efficiency for the loops in the *eco1-W216G* mutant. We found that the cross-linking

efficiency for both the 35S (primers R7 and R6) and the 5S (R2 and R4) loops was significantly lower in the *eco1-W216G* mutant (Figure 3C). The cross-linking efficiency for a primer pair in the rDNA that does not detect a loop (R7 and F4) showed no difference between the WT and mutant and was used for normalization. In addition, the cross-linking efficiency for a primer pair on chromosome VI did not show any difference between WT and mutant (unpublished data), further suggesting a locus-specific effect. Our results support the idea that rDNA architecture partly depends on the acetylation activity of Eco1. The acetylated form of the cohesin complex may contribute to the efficient production of RNA from the 35S gene loop.

Mutations in cohesin ring subunits cause defects in ribosome biogenesis

We previously demonstrated defects in ribosome biogenesis in yeast and human cells with the *eco1-W216G* mutation (Bose *et al.*, 2012). We asked whether defects in ribosome biogenesis are found in other cohesin mutants. We used ribosomal protein green fluorescent protein (GFP) reporter plasmids to test the aberrant accumulation of ribosomal proteins in strains with mutations in the cohesin ring (Figure 4). Normally Rps2-GFP (small 40S subunit) and Rpl25-GFP (large 60S subunit) are evenly distributed in the cytoplasm, but an assembly or export defect will cause them to accumulate in bright foci in the nucleus or nucleolus (Hurt *et al.*, 1999; Li *et al.*, 2009). Several commonly used temperature-sensitive mutants were tested at 30°C, including *irr1-1*, *mcd1-73*, *smc1-259*, and *smc3-1*. We collected images to visualize GFP (Figure 4, A and B), as well as cytometry to quantify peak fluorescence (Figure 4, C–F). We found that mutations in any subunit of the cohesin ring show defects compared with WT, as did *eco1-W216G* (Bose *et al.*, 2012), arguing that defects in ribosome biogenesis are a general feature of cohesin mutant strains.

Cohesion at the rDNA establishes and maintains nucleolar morphology

The *eco1-W216G* mutant exhibits a mild reduction in cohesion at centromeres, chromosomes arms, and telomeres (Lu *et al.*, 2010) and a more significant reduction at rDNA (Bose *et al.*, 2012), despite the fact that cohesin still associates with chromosomes in a normal pattern (Gard *et al.*, 2009). Although this mutation is associated with nucleolar defects, it is also associated with hundreds of changes in gene expression, raising the possibility that the nucleolar defect is an indirect consequence of the altered gene expression program (Bose *et al.*, 2012). We wanted to know whether formation of the nucleolus required cohesion. We explored nucleolar structure in a

independent reactions. Error bars, SE. *$p < 0.05$ by a two-tailed *t* test. (C) Chromatin fractionation was performed using three independent biological replicates, and the amount of rDNA in the high-speed fraction was quantified for WT and *eco1-W216G* mutant strains using qPCR and the primers shown in B. Values for the *eco1-W216G* strain are shown with respect to WT, which was normalized to 1. There is no significant difference according to a two-tailed *t* test. (D) Strains were grown in YPD + 1 M sorbitol at 30°C. The number of polymerases (pols) per active 35S gene was quantified in Miller spreads: *eco1-W216G* mutant strain, average 41 pols/gene, SD = 16, *n* = 182, 68% of genes are active, 39 DNA strands, 172 total genes, W303a, average 50 pols/gene, SD = 16, *n* = 113, 61% of genes are active, 19 DNA strands, 80 total genes. For visual clarity, a nonoverlapping gene on a parallel chromatin strand was removed from the image of the WT gene. Scale bar, 0.2 μm. For BY4742 there were average 52 pols/gene, SD = 16, *n* = 286, 81% of genes are active, 252 total genes on 62 DNA strands, and for the *eco1-W216G* strain there were average 56 pols/gene, SD = 21, *n* = 272, 77% of genes active, 187 total genes on 40 DNA strands. (E) Strains with a unique sequence inserted into one rDNA repeat were monitored for transcript production by FISH (Tan and van Oudenaarden, 2010; Bose *et al.*, 2012). For each strain, at least two independent cultures were monitored and at least 300 total cells were quantified. Cells were binned based on the number of transcripts per cell. The distribution for WT vs. either the *rpa49* or *eco1-W216G* mutant was tested for significance using a two-tailed Student's *t* test with a result of $p < 0.001$ in both cases. The data for WT and *eco1-W216G* strains were previously reported (Bose *et al.*, 2012).
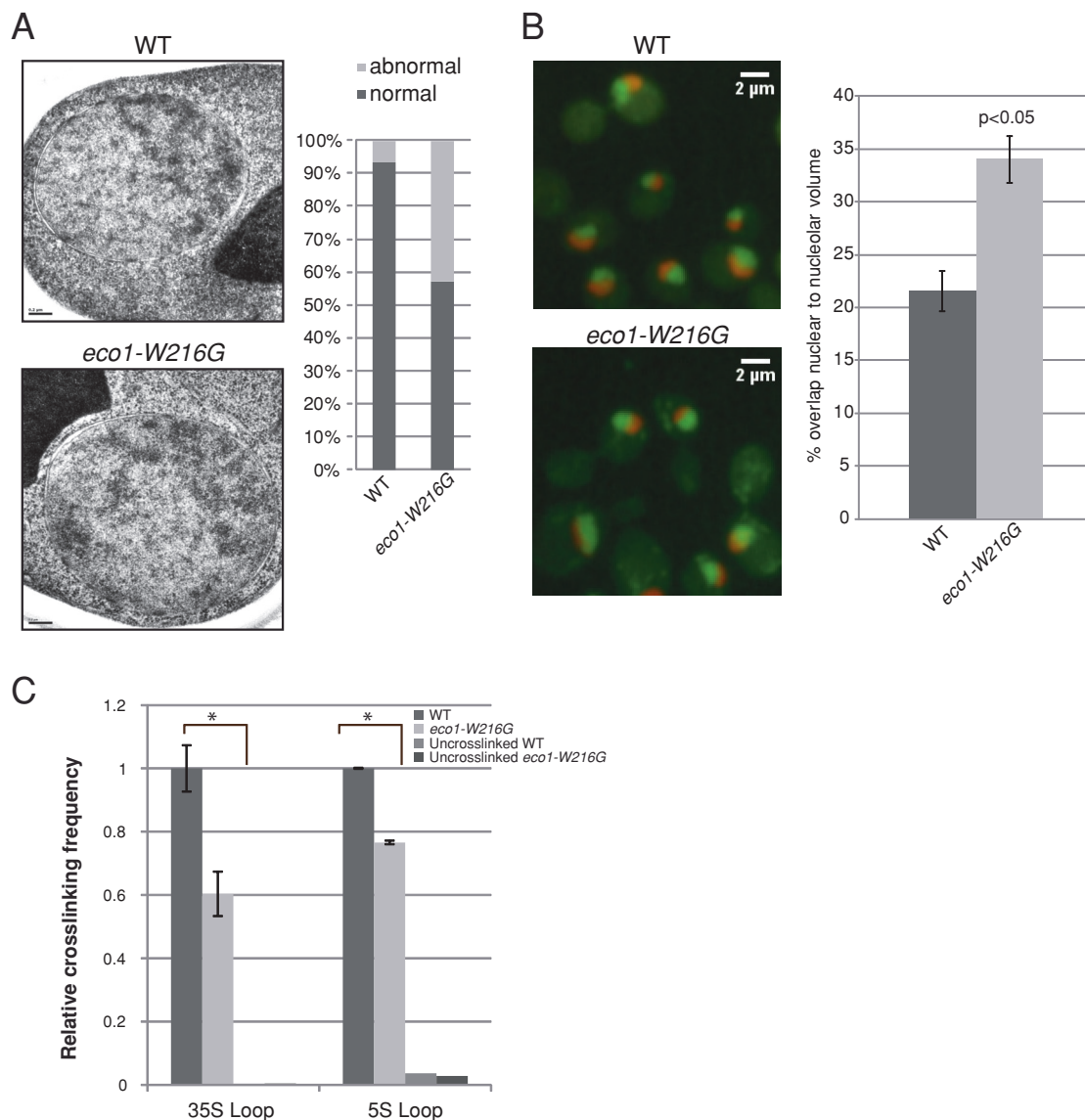
FIGURE 3: Nucleolar morphology and rDNA looping are disrupted in the *eco1-W216G* mutant. (A) Asynchronous cultures were grown in YPD, and 28–30 nucleoli were examined for each strain by transmission electron microscopy. Both samples contained nuclei without detectable nucleoli. Undetectable or dispersed nucleoli not having a compact crescent shape were scored as abnormal. (B) Cells containing the nucleolar protein Sik1-RFP were grown in YPD and arrested in G2/M with nocodazole. Cells were fixed with 4% paraformaldehyde and resuspended in mounting medium containing DAPI. One hundred cells from two biological replicates were counted for each strain. Scoring is described in *Materials and Methods*. (C) For 3C, un-cross-linked DNA was used as a negative control. Primers pairs were used to detect the 35S loop, the 5S loop, and a random primer pair in the rDNA. The values for 35S and 5S primer pairs were normalized to the values obtained for the random primer pair in the rDNA, which does not show any difference between strains. Data from two independent biological replicates are shown. Error bars, SE from PCRs performed in triplicate. A paired *t* test was performed; *$p < 0.05$.

single cell cycle in the event that 1) cohesion was not established or 2) cohesion was prematurely destroyed in metaphase. For the first condition, we used a strain in which the sole copy of Mcd1 was under the control of the GAL_{1-10} promoter (Figure 5A). Although this strain can grow in the presence of galactose, it is unable to grow on dextrose. We arrested the strain in G1 with α-factor and then maintained the arrest for an additional 1 h either in galactose or dextrose. Mcd1 is depleted in dextrose relative to galactose. After G1 arrest, we released the cells into the cell cycle and allowed replication to occur. The dextrose culture lacks cohesion. We then analyzed the nucleolus by EM. Whereas most of the nucleoli in the galactose

culture looked normal, the nucleoli for the dextrose culture were highly abnormal. This experiment shows that when cohesion is not established during S phase, the nucleolar morphology is aberrant.

To test whether cohesion would be required to maintain nucleolar structure in G2/M, we used a strain in which the sole copy of Mcd1 contains a tobacco etch virus (TEV) protease cleavage site (Figure 5B). The expression of TEV protease is controlled by the GAL_{1-10} promoter. The strain was grown in raffinose and arrested with nocodazole, and then either dextrose or galactose was added for 2 h along with more nocodazole to maintain the G2/M arrest. The overlap of Sik1-RFP and DAPI was quantified in the two conditions.
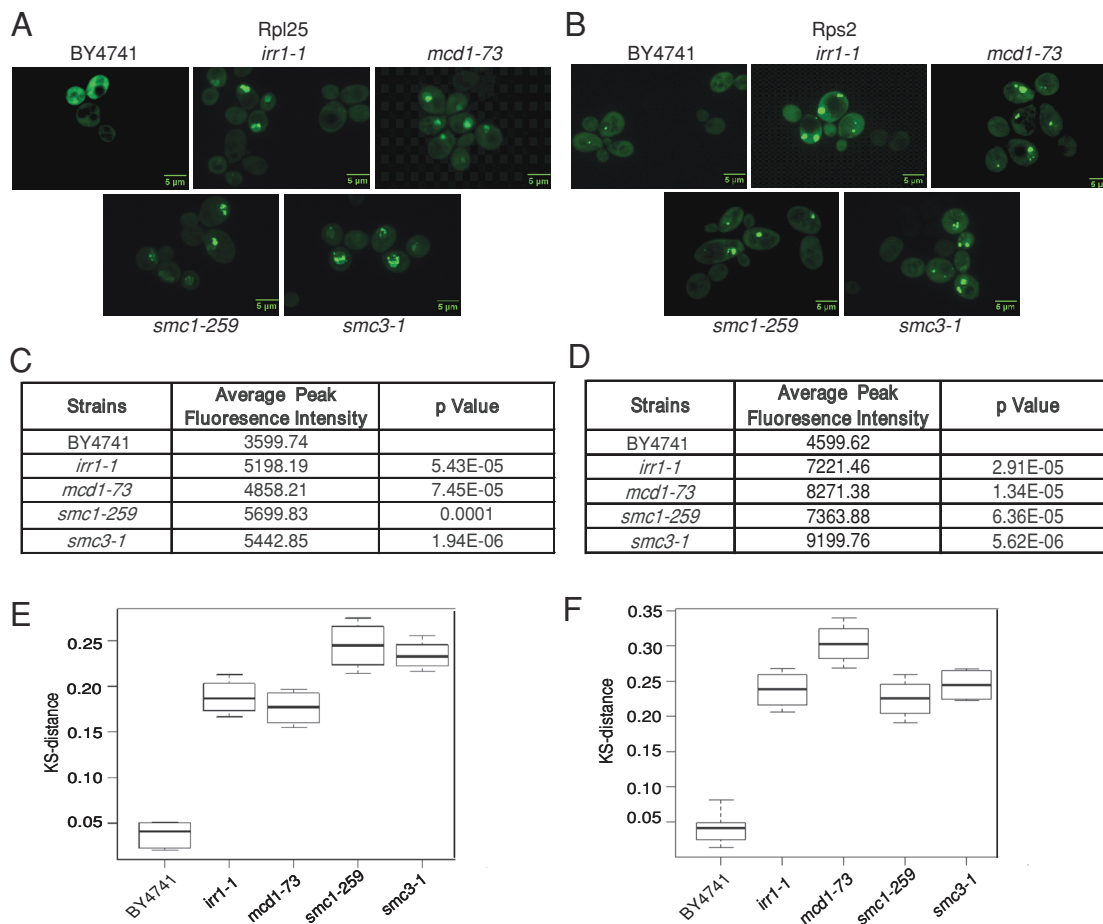
FIGURE 4: Mutations in cohesin ring subunits show defects in 40S and 60S ribosome biogenesis. The cohesin mutant strains and WT control (BY4741) were transformed with 60S ribosome subunit reporter plasmid, Rpl25-GFP-URA3 (A), or 40S ribosome subunit reporter, Rps2-GFP-LEU2 (B). Cells were grown in standard defined (SD)-Ura broth (A) or SD-Leu broth (B) at 30°C to mid log phase. Live-cell images were collected using confocal microscopy (Ultraview Spinning Disc) with 100×/1.45 NA Plan-Apochromat oil objective and an ORCA-R2 camera and analyzed by Volocity and ImageJ software. For quantitative analysis, peak GFP fluorescence for 10,000 cells was measured by cytometry using two independent isolates, and the average peak intensity is shown (C, D). A Kolmogorov-Smirnov (KS) test was applied to the distribution of peak GFP fluorescence, and the distance of each mutant from WT is shown using a box plot (E, F) with p values from the KS test (C, D).

We found that there was significantly more overlap in the condition under which cohesin was cleaved with TEV protease, similar to what was observed for the *eco1-W216G* mutant. This result suggests that cohesion is needed to maintain the separation between bulk chromatin and the nucleolus and helps to organize the rDNA into the nucleolus.

A number of mutations have been identified in cohesin genes that result in a spectrum of human diseases termed cohesinopathies (Liu and Krantz, 2008). Cornelia de Lange syndrome is caused by mutations in Smc1, Smc3 (Deardorff *et al.*, 2007), Scc2/Nipbl (Krantz *et al.*, 2004; Tonkin *et al.*, 2004), and Hdac8/Hos1 genes (Deardorff *et al.*, 2012a), and a related syndrome is caused by mutations in Rad21/Mcd1/Scc1 (Deardorff *et al.*, 2012b). Mutations in the cohesin acetyltransferase, ESCO2 (*ECO1* in yeast), are associated with RBS (Vega *et al.*, 2005). In these syndromes, chromosome segregation is relatively unimpaired. However, the gene expression landscape is altered. Disease mutations in *SMC1* and *ECO1* genes in budding yeast and the ESCO2 gene in human cells affect translation (Bose *et al.*, 2012). Furthermore, mutations in cohesin are associated with myeloid neoplasms (Kon *et al.*, 2013; Ley *et al.*, 2013). Here we

demonstrate faulty nucleolar structure and function when cohesion is defective. Combined with previous findings, we hypothesize that the lack of nucleolar organization that occurs when cohesion is compromised results in defects in rRNA production, as well as in other transcriptional changes. Nucleolar organization in mammalian cells contributes not only to Pol I transcription, but also to Pol III transcription and to repression of perinucleolar heterochromatin (Nemeth *et al.*, 2010; van Koningsbruggen *et al.*, 2010; Fedoriw *et al.*, 2012). Cohesion within the rDNA may normally help to organize the nucleolus and coordinate expression of nucleolar-associated sequences.

MATERIALS AND METHODS
All strains are listed in Supplemental Table S1.

Transmission electron microscopy
Cultures were grown in 200 ml of yeast extract/peptone/dextrose (YPD) to an OD_{600} of ~0.8. Samples were frozen on the EM-Pact (Leica) at ~2050 bar, transferred under liquid nitrogen into 2% osmium tetroxide/0.1% uranyl acetate/acetone/2% water, and then transferred to the Leica AFS2. The freeze-substitution protocol
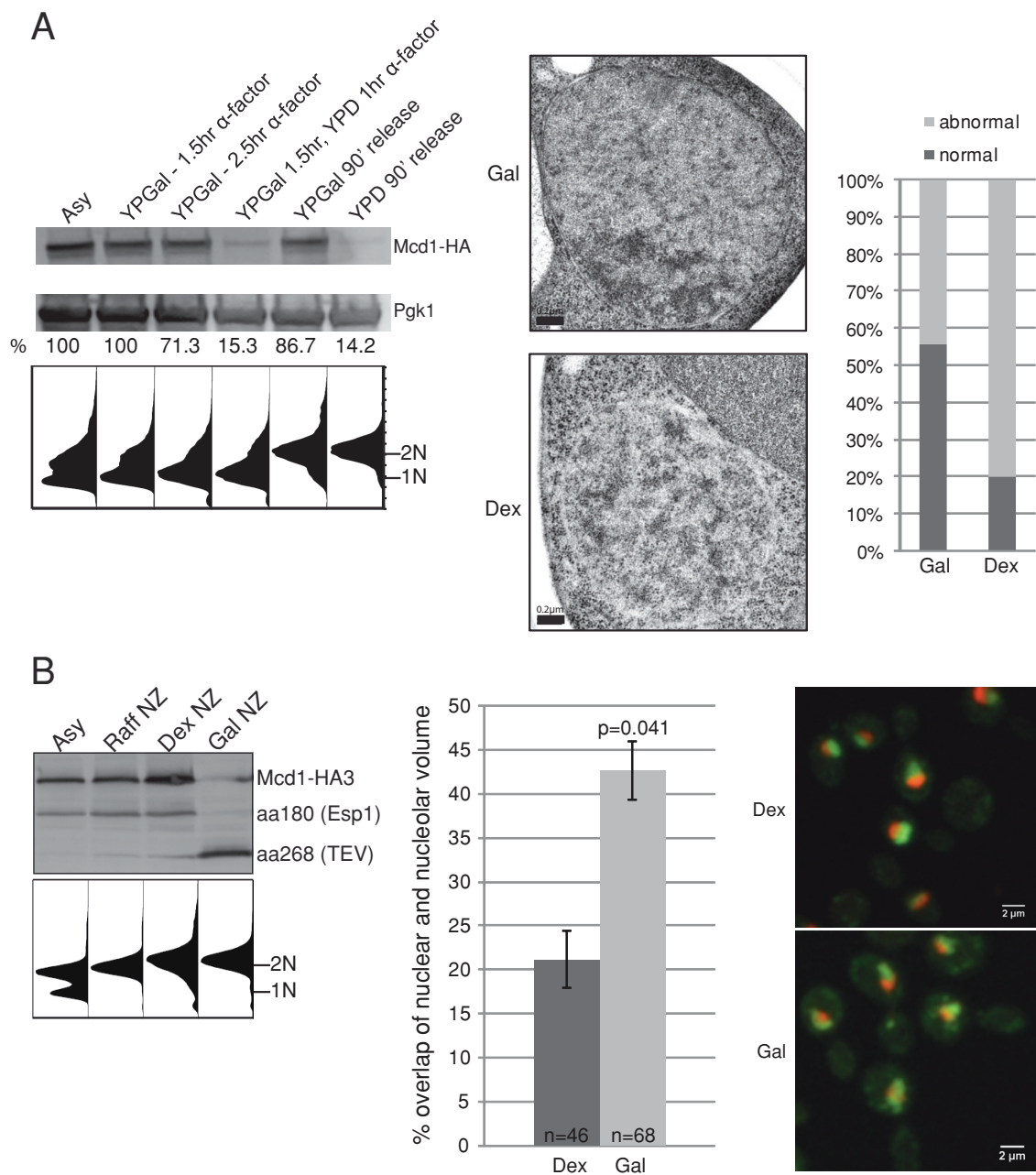
FIGURE 5: Cohesion is necessary for nucleolar integrity. (A) A culture was grown in YP/galactose and then treated with α-factor for 1.5 h. The culture was split in half, with one culture transferred to YPD. The α-factor treatment was maintained for another hour. Each culture was released for 90 min, and cells were collected for electron microscopy. For the Western blot, equal amounts of protein from whole-cell extracts were loaded to monitor Mcd1-HA and Pgk1 as a loading control. The level of Mcd1 is shown as a percentage of the Pgk1 signal. The cytometric analysis of the cultures is shown below the Western blot. Nucleoli were scored as in Figure 3; 20 of 36 in galactose looked normal, and 4 of 20 in dextrose looked normal. (B) A culture was grown in YP/raffinose and arrested with nocodazole. The culture was split, maintaining the nocodazole arrest for 2 h, with half receiving dextrose and half receiving galactose to induce the TEV protease. For the Western blot, equal amounts of protein from whole-cell extracts were loaded to monitor the cleavage of Mcd1-HA by Esp1 or TEV protease. The cytometric analysis of the cultures is shown below the Western blot. The percentage overlap between the Sik1-RFP signal and the DAPI signal was scored as in Figure 3.

started samples at −90°C for 72 h, up 5°C/h, −20°C for 12 h, up 5°C/h, to 0°C for 5 h. Samples were then removed from the AFS2 and allowed to come to room temperature for 1 h before going through three changes of acetone over 1 h. They were removed from the planchettes and stepwise embedded in acetone/Epon/Araldite mixtures to the final 100% Epon/Araldite over several days. Sections were then cut at 80 nm on a Leica UC6, stained

with uranyl acetate and Sato's lead, and imaged on a Tecnai Spirit (FEI).

ChIP-qPCR

Cells were grown to an OD_{600} of ~0.6, fixed in 1% formaldehyde for 15 min, and then quenched with glycine (final concentration 0.125 M) for 5 min. Cells were frozen, then lysed for 1 h at 4° in

FA-lysis buffer (50 mM 4-(2-hydroxyethyl)-1-piperazineethanesulfonic acid, pH 7.5, 150 mM NaCl, 1 mM EDTA, 1% Triton X-100, 0.1% sodium deoxycholate). The lysate was sonicated using a Biorupter for 30 min, 30 s on/off, at medium intensity. Protein concentration was normalized after chromatin shearing and before proceeding with the immunoprecipitation. A 2.5-μl amount of anti-FLAG antibody (F3165; Sigma) was added to 400 μl of chromatin extract and incubated at 4°C overnight. A 50-μl amount of Protein G Dynabeads (100-04D; Invitrogen) was added and incubated at 4°C for 2 h, then washed with FA-lysis buffer, twice in FA-lysis buffer with 500 mM NaCl, TEL buffer (0.25 M LiCl, 10 mM Tris-HCl, pH 8.0, 1 mM EDTA, 1% NP-40, 1% sodium deoxycholate), and then twice with 1× TE (10 mM Tris-HCl, pH 8.0, 1 mM EDTA). Chromatin fragments were eluted by adding 200 μl of elution buffer (1% SDS, 250 mM NaCl, TE) and shaking the beads at 65°C. Two elutions were combined and treated with Proteinase K for 1 h at 55°C. Cross-linking was reversed, and the DNA was extracted and precipitated. qPCR was performed in triplicate using a Perfecta SYBR Green FastMix (Quanta Biosciences). Primer sequences for rDNA are listed in Supplemental Table S2.

Chromatin fractionation

This method was performed as previously described (Rougemaille et al., 2008). Cells were grown, cross-linked, and lysed according to the ChIP method. After lysis, the lysate was transferred to a 2-ml tube, put at 4°C, and rotated for 2 h. The lysate was then spun down for 20 min at 4°C at 12,000 rpm. The resulting chromatin pellet was resuspended in 1.8 ml of FA-lysis buffer and sonicated according to the ChIP method. The sheared chromatin was then rotated at 4°C for 30 min and then divided into two aliquots. One aliquot was spun at 4°C for 15 min at 2000 × g, and the other aliquot was spun at 4°C for 15 min at 18,000 × g. Both pellets were resuspended in 100 μl of FA-lysis buffer. All samples were then treated with Proteinase K, cross-links were reversed. and DNA was extracted as in the ChIP method. DNA pellets were resuspended in 100 μl of 1× TE buffer and concentrations determined. Equal amounts of DNA were used, and qPCR was performed as in the ChIP method.

Miller spreads

Miller spreads, polymerase counts, and determination of percentage of active genes were performed as previously described (French et al., 2003), with the exception that the spreads were not rotary shadow-cast with platinum.

3C

The 3C method for rDNA was performed as previously described (Mayan and Aragon, 2010).

Sik1-RFP imaging and analysis

For Figure 2, images were collected using confocal microscopy (Ultraview Spinning Disc; PerkinElmer) with a 100×/1.45 numerical aperture (NA) Plan Apochromat oil objective, along with a 405/488/561/640–nm dichroic. Emission was collected with a Orca-R2 camera (Hamamatsu), RFP through a 420-475/502-544/582-618/663-691–nm multi–band pass emission filter and DAPI through a 415-475/580-650–nm dual–band pass emission filter. Excitation at 405 nm (DAPI) and 561 nm (RFP) was alternated to limit cross-talk. For Figure 4, microscopy images were obtained with the APD imaging module of a Confocor3 (Zeiss) using a 63×/1.4 NA Plan Apochromat oil objective with a 405/488/561–nm main dichroic. DAPI and RFP emission were collected through 420- to 475-nm and LP 580-nm filters, respectively. Excitation at 405 nm (DAPI) and 561 nm (RFP) was alternated in multitrack mode to eliminate cross-talk. The

pinhole was set at 1.0 Airy unit. In both cases Z-slices were acquired with 0.5-μm steps. Pixel size was 60 nm.

Overlap between DAPI and nucleolar signals was estimated using custom macros and plug-ins written in ImageJ (National Institutes of Health, Bethesda, MD). First, background intensity was subtracted by manually selecting a region away from cells and subtracting its average from every image in the three-dimensional (3D) stack. Next, each image slice was Gaussian smoothed with a SD of 3 pixels. The resulting image was thresholded in three dimensions at a fraction of the maximum smoothed 3D intensity. This threshold was chosen for each sample as the level at which spots were segmented fully without segmenting regions outside cells. The resulting masks were replaced with the z-dimension size and summed to obtain the integrated z-volumes for each pixel. Overlapping regions were summed in a similar manner. Spots with areas of <15 pixels were assumed to be noise. DAPI and nucleolar masks were combined and dilated twice to obtain nuclear masks. As a result, spots separated by >4 pixels were considered to be in separate nuclei. Finally, DAPI, nucleolar, and overlapping volumes within each nucleus were integrated.

Cytometric quantification and analysis of peak GFP fluorescence

This method was performed as previously described (Bose et al., 2012).

FISH

FISH was performed as previously described (Tan and van Oudenaarden, 2010; Bose et al., 2012). rRNA count distributions were fitted to models assuming first-order gene activation/inactivation (α/γ). rRNA production (μ) and degradation (δ) rates were calculated in a similar manner to that of Tan and van Oudenaarden (2010) and expressed in units of the degradation rate. The size of each burst (in numbers of rRNA molecules), given by μ/γ, remains essentially constant for all possible fit combinations. The δ is assumed to be constant. To calculate error, we used Monte Carlo simulation of the best fit with random errors corresponding to our data error level and then fitted the simulated data. The simulation and fit process was repeated 100 times with a fixed μ. The reported error is the SD of the burst size from 100 simulated fits.

REFERENCES

Albert B, Leger-Silvestre I, Normand C, Ostermaier MK, Perez-Fernandez J, Panov KI, Zomerdijk JC, Schultz P, Gadal O (2011). RNA polymerase I-specific subunits promote polymerase clustering to enhance the rRNA gene transcription cycle. J Cell Biol 192, 277–293.

Beckouet F, Labarre-Mariotte S, Albert B, Imazawa Y, Werner M, Gadal O, Nogi Y, Thuriaux P (2008). Two RNA polymerase I subunits control the binding and release of Rrn3 during transcription. Mol Cell Biol 28, 1596–1605.

Bose T et al. (2012). Cohesin proteins promote ribosomal RNA production and protein translation in yeast and human cells. PLoS Genet 8, e1002749.

Bose T, Gerton JL (2010). Cohesinopathies, gene expression, and chromatin organization. J Cell Biol 189, 201–210.

Deardorff MA *et al.* (2007). Mutations in cohesin complex members SMC3 and SMC1A cause a mild variant of cornelia de Lange syndrome with predominant mental retardation. Am J Hum Genet 80, 485–494.

Deardorff MA *et al.* (2012a). HDAC8 mutations in Cornelia de Lange syndrome affect the cohesin acetylation cycle. Nature 489, 313–317.

Deardorff MA *et al.* (2012b). RAD21 mutations cause a human cohesinopathy. Am J Hum Genet 90, 1014–1027.

Fedoriw AM, Starmer J, Yee D, Magnuson T (2012). Nucleolar association and transcriptional inhibition through 5S rDNA in mammals. PLoS Genet 8, e1002468.

French SL, Osheim YN, Cioci F, Nomura M, Beyer AL (2003). In exponentially growing *Saccharomyces cerevisiae* cells, rRNA synthesis is determined by the summed RNA polymerase I loading rate rather than by the number of active genes. Mol Cell Biol 23, 1558–1568.

Gard S, Light W, Xiong B, Bose T, McNairn AJ, Harris B, Fleharty B, Seidel C, Brickner JH, Gerton JL (2009). Cohesinopathy mutations disrupt the subnuclear organization of chromatin. J Cell Biol 187, 455–462.

Ghosh S *et al.* (2012). Acetylation of the SUN protein Mps3 by Eco1 regulates its function in nuclear organization. Mol Biol Cell 23, 2546–2559.

Guacci V, Koshland D, Strunnikov A (1997). A direct link between sister chromatid cohesion and chromosome condensation revealed through the analysis of MCD1 in *S. cerevisiae*. Cell 91, 47–57.

Heidinger-Pauli JM, Mert O, Davenport C, Guacci V, Koshland D (2010). Systematic reduction of cohesin differentially affects chromosome segregation, condensation, and DNA repair. Curr Biol 20, 957–963.

Hurt E, Hannus S, Schmelzl B, Lau D, Tollervey D, Simos G (1999). A novel in vivo assay reveals inhibition of ribosomal nuclear export in ran-cycle and nucleoporin mutants. J Cell Biol 144, 389–401.

Kirkland JG, Kamakaka RT (2013). Long-range heterochromatin association is mediated by silencing and double-strand DNA break repair proteins. J Cell Biol 201, 809–826.

Kon A *et al.* (2013). Recurrent mutations in multiple components of the cohesin complex in myeloid neoplasms. Nat Genet 45, 1232–1237.

Kos M, Tollervey D (2010). Yeast pre-rRNA processing and modification occur cotranscriptionally. Mol Cell 37, 809–820.

Krantz ID *et al.* (2004). Cornelia de Lange syndrome is caused by mutations in NIPBL, the human homolog of *Drosophila melanogaster* Nipped-B. Nat Genet 36, 631–635.

Laferte A, Favry E, Sentenac A, Riva M, Carles C, Chedin S (2006). The transcriptional activity of RNA polymerase I is a key determinant for the level of all ribosome components. Genes Dev 20, 2030–2040.

Laloraya S, Guacci V, Koshland D (2000). Chromosomal addresses of the cohesin component Mcd1p. J Cell Biol 151, 1047–1056.

Ley TJ *et al.* (2013). Genomic and epigenomic landscapes of adult de novo acute myeloid leukemia. N Engl J Med 368, 2059–2074.

Li Z, Lee I, Moradi E, Hung NJ, Johnson AW, Marcotte EM (2009). Rational extension of the ribosome biogenesis pathway using network-guided genetics. PLoS Biol 7, e1000213.

Liu J, Krantz ID (2008). Cohesin and human disease. Annu Rev Genomics Hum Genet 9, 303–320.

Lu S, Goering M, Gard S, Xiong B, McNairn AJ, Jaspersen SL, Gerton JL (2010). Eco1 is important for DNA damage repair in *S. cerevisiae*. Cell Cycle 9, 3315–3327.

Mayan M, Aragon L (2010). *Cis*-interactions between non-coding ribosomal spacers dependent on RNAP-II separate RNAP-I and RNAP-III transcription domains. Cell Cycle 9, 4328–4337.

Narla A, Ebert BL (2010). Ribosomopathies: human disorders of ribosome dysfunction. Blood 115, 3196–3205.

Nemeth A *et al.* (2010). Initial genomics of the human nucleolus. PLoS Genet 6, e1000889.

Nemeth A, Langst G (2011). Genome organization in and around the nucleolus. Trends Genet 27, 149–156.

Osheim YN, French SL, Keck KM, Champion EA, Spasov K, Dragon F, Baserga SJ, Beyer AL (2004). Pre-18S ribosomal RNA is structurally compacted into the SSU processome prior to being cleaved from nascent transcripts in *Saccharomyces cerevisiae*. Mol Cell 16, 943–954.

Rolef Ben-Shahar T, Heeger S, Lehane C, East P, Flynn H, Skehel M, Uhlmann F (2008). Eco1-dependent cohesin acetylation during establishment of sister chromatid cohesion. Science 321, 563–566.

Rougemaille M *et al.* (2008). THO/Sub2p functions to coordinate 3′-end processing with gene-nuclear pore association. Cell 135, 308–321.

Schaaf CA, Kwak H, Koenig A, Misulovin Z, Gohara DW, Watson A, Zhou Y, Lis JT, Dorsett D (2013). Genome-wide control of RNA polymerase II activity by cohesin. PLoS Genet 9, e1003382.

Schneider DA, Michel A, Sikes ML, Vu L, Dodd JA, Salgia S, Osheim YN, Beyer AL, Nomura M (2007). Transcription elongation by RNA polymerase I is linked to efficient rRNA processing and ribosome assembly. Mol Cell 26, 217–229.

Tan RZ, van Oudenaarden A (2010). Transcript counting in single cells reveals dynamics of rDNA transcription. Mol Syst Biol 6, 358.

Tonkin ET, Wang TJ, Lisgo S, Bamshad MJ, Strachan T (2004). NIPBL, encoding a homolog of fungal Scc2-type sister chromatid cohesion proteins and fly Nipped-B, is mutated in Cornelia de Lange syndrome. Nat Genet 36, 636–641.

Unal E, Heidinger-Pauli JM, Kim W, Guacci V, Onn I, Gygi SP, Koshland DE (2008). A molecular determinant for the establishment of sister chromatid cohesion. Science 321, 566–569.

van Koningsbruggen S, Gierlinski M, Schofield P, Martin D, Barton GJ, Ariyurek Y, den Dunnen JT, Lamond AI (2010). High-resolution whole-genome sequencing reveals that specific chromatin domains from most human chromosomes associate with nucleoli. Mol Biol Cell 21, 3735–3748.

Vega H *et al.* (2005). Roberts syndrome is caused by mutations in ESCO2, a human homolog of yeast ECO1 that is essential for the establishment of sister chromatid cohesion. Nat Genet 37, 468–470.

Xu B, Lee KK, Zhang L, Gerton JL (2013). Stimulation of mTORC1 with L-leucine rescues defects associated with Roberts syndrome. PLoS Genet 9, e1003857.

Zhang Y, Wen Z, Washburn MP, Florens L (2010). Refinements to label free proteome quantitation: how to deal with peptides shared by multiple proteins. Anal Chem 82, 2272–2281.